scientific reports

OPEN

Solvent extraction of Ac-225 in nano-layer coated, solvent resistant PDMS microfluidic chips

Svenja Trapp[1,4], Albert Santoso[2,4], Yassine Hounat[2], Elisabeth Paulssen[1,3], J. Ruud van Ommen[2], Volkert van Steijn[2✉] & Robin M. de Kruijff[1✉]

Separating medical radionuclides from their targets is one of the most critical steps in radiopharmaceutical production. Among many separation methods, solvent extraction has a lot of potential due to its simplicity, high selectivity, and high efficiency. Especially with the rise of polydimethylsiloxane (PDMS) microfluidic chips, this extraction process can take place in a simple and reproducible chip platform continuously and automatically. Furthermore, the microfluidic chips can be coated with metal-oxide nano-layers, increasing their resistance against the employed organic solvents. We fabricated such chips and demonstrated a parallel flow at a considerably large range of flow rates using the aqueous and organic solutions commonly used in medical radionuclide extraction. In our following case study for the separation of Ac-225 from radium with the chelator di(2-ethylhexyl) phosphoric acid (D2EHPA), a remarkable extraction efficiency of 97.1 % $\pm$ 1.5 % was reached within 1.8 seconds of contact time, while maintaining a near perfect phase separation of the aqueous and organic solutions. This method has the potential to enable automation of solvent extraction and faster target recycling, and serves, therefore, as a proof-of-concept for the applicability of microfluidic chip solvent extraction of (medical) radionuclides.

Keywords Microfluidics, Solvent extraction, PDMS, Parallel flow, Medical radionuclides, Ac-225

In nuclear medicine, radionuclides are utilized for imaging and treatment of various diseases[1]. Despite numerous existing potential radionuclides, only a handful reach clinical use, partly due to their limited availability[2,3]. Increasing the global supply requires a production system that is not only fast and efficient, but also continuous and automatable, incorporating the necessary steps to separate the produced radionuclide from its initial target material[2,4]. Solvent extraction, among other methods, offers a simple, selective, and efficient means of separation[5]. By bringing an aqueous solution that contains the product radionuclide as well as its target material in contact with an immiscible organic solution that contains a chelator, the chelator selectively binds to the product radionuclide[5,6]. As a result, the product radionuclide gets extracted into the organic solution, while the valuable target material stays in the aqueous solution, potentially ready to be recycled. To prepare the product radionuclide for further use, it needs to be transferred to a fresh aqueous solution, which is possible through a simple second (back-) extraction step. Microfluidic devices offer precise control over two-phase flows and their interfaces, enabling the design of a continuous and potentially automatable extraction system[7–12]. With short diffusion paths, these devices consistently achieve high extraction efficiencies for many radionuclides[9].

Polydimethylsiloxane (PDMS), among the most used materials for microfluidic devices stands out as it (1) allows rapid prototyping through a simple molding technique[13], (2) has a high radiation resistance as opposed to commercial membranes used for radionuclide separation[14], and (3) resists solution with extreme pH used in the (back-) extraction step for the separation of medical radionuclides[15–17]. Furthermore, PDMS has also been used in medical industries, easily complying with regulatory demands[15]. The only downside is that it swells and deforms when it comes in contact with organic solutions commonly used for extraction[18]. To overcome this issue, direct contact between the organic solution and the PDMS microfluidic chip must be prevented. Recently, we developed a simple approach to coat the channels of PDMS chips with metal oxide nano-layers using atomic layer deposition (ALD)[17]. These nano-layers are grown by alternately flowing the two gaseous ALD reactants through the chips, a metal precursor and an oxidizing agent, with a purge of inert gas in between. The number of repeats allows high control over the layer thickness and its properties due to the self-limiting nature of the ALD

[1]Department of Radiation Science and Technology, Delft University of Technology, 2629 JB Delft, the Netherlands. [2]Department of Chemical Engineering, Delft University of Technology, 2629 HZ Delft, the Netherlands. [3]Department of Chemistry and Biotechnology, Aachen University of Applied Science, 52428 Jülich, Germany. [4]Svenja Trapp and Albert Santoso contributed equally to this work. ✉email: v.vansteijn@tudelft.nl; r.m.dekruijff@tudelft.nl

reactions[19]. This invention now opens the door to develop a PDMS-based microfluidic system for radionuclide solvent extraction.

In this study, we present a PDMS-based microfluidic radionuclide extraction system, in which the PDMS is rendered inert against the use of organic solutions through a silicon oxide nano-layer deposited by means of ALD. Besides the nano-layer, a second important feature of the microfluidic chip is the difference in height between the channels for the organic phase containing the chelator and the aqueous phase containing the product radionuclide and its target material, see Fig. 1. The height difference ensures pinning of the interface[20], securing stable parallel flow, even at the lowest flow rates. A third important feature is the wavy-wall near the exit, securing that the interface remains pinned, achieving perfect phase separation. As a proof of concept, we present a case study for the separation of actinium-225 (Ac-225) from radium, using di-2-ethylhexylphosphoric acid (D2EHPA) as the chelator, after initial experiments on the separation of lanthanum-140 (La-140) from barium as substitutes. Ac-225 is a medical radionuclide, that decays through a series of radioactive daughter nuclides to relatively stable bismuth-209 (Bi-209), emitting a total of 4 alpha (α)-particles in its decay chain. It is currently researched for targeted alpha therapy, showing very promising clinical results[21-23]. However, so far, the global supply of Ac-225 is severely limited and does not meet the predicted clinical demand[3]. Therefore, many efforts are made to produce Ac-225 via a plethora of different production routes[24], including proton irradiation of radium-226 (Ra-226) targets through the ^{226}Ra(p,2n)^{225}Ac reaction or photon irradiation of Ra-226 leading to ^{226}Ra(γ,n)^{225}Ra $\rightarrow$ ^{225}Ac[3,25-27]. The presented case study showcases a fast, continuous, and efficient process using microfluidic solvent extraction, with the potential for establishing an automated purification system for medical radionuclides.

Methods and materials
Microfluidic device
Working principle of the microfluidic device design
Two key requirements for continuous two-phase flow extraction are that the two phases (1) flow stably side by side through the main channel, without breaking up into slugs, and (2) leave the device separately via the two dedicated outlet channels. To accommodate these requirements, we adapted the geometry often used in solvent extraction[5], namely a simple straight channel (500 µm wide and 11.6 mm long in our work) with a Y-junction for the introduction of the two phases and another Y-junction for their exit. Two important geometries were added to pin the interface throughout the device: a vertical guiding structure in the form of a step height[20,28] and a lateral guiding structure in the form of a wavy wall at the outlet junction, see Fig. 1. The position of the step height in the main channel is determined by the estimated interface position of the two fluids. Assuming two-dimensional flow and considering continuity of velocity and shear stress, the interface position is a function of the viscosity ratio and the flow rate ratio[29-31]. In this study, the viscosities of the fluids used for the radionuclide separations are of a comparable order of magnitude. Additionally, extraction is done at comparable flow rates. Therefore, the step height is placed in the middle of the main channel to account for most of the used operating
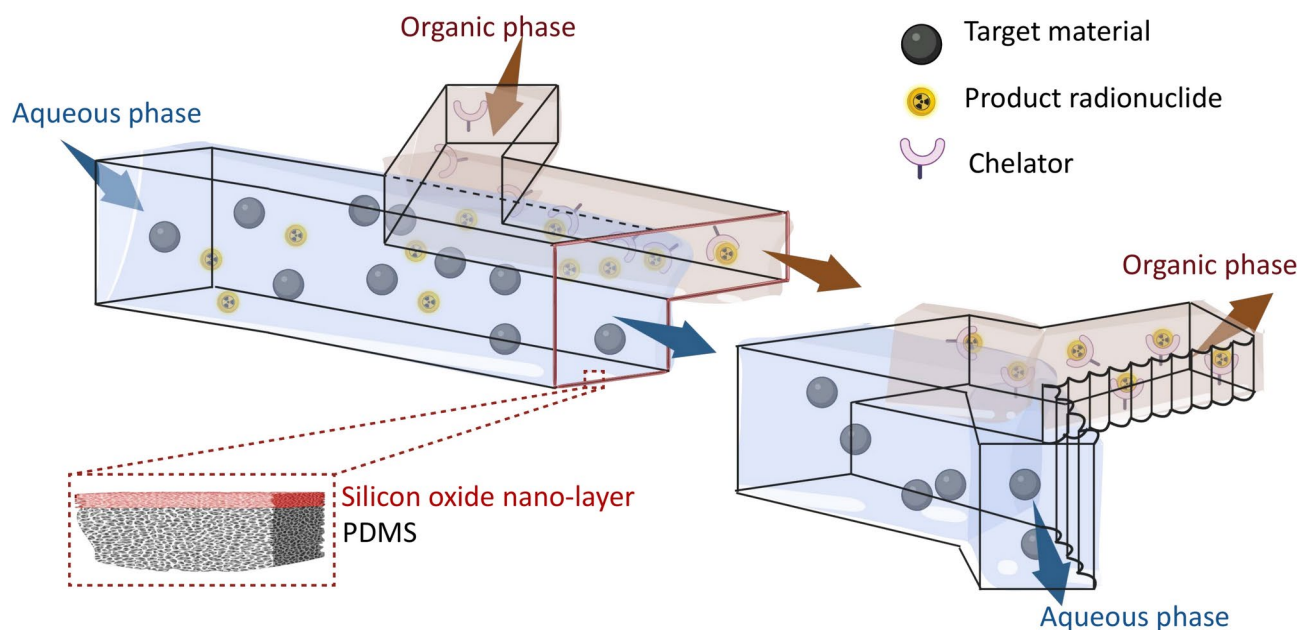

Fig. 1. Illustration of continuous two-phase liquid-liquid extraction of radionuclides in a PDMS-based microfluidic chip, with the product radionuclide and its target supplied in the aqueous phase and the chelator in the organic phase. The silicon oxide nano-layer coated on the walls using atomic layer deposition renders the wall inert against the organic phase. The difference in height between the side where aqueous phase and the organic phase flow ensures pinning of the interface, ensuring stable parallel flow. The wavy wall near the exit pins the interface as well, ensuring perfect phase separation.

conditions. The channel for the aqueous phase was 100 μm deep, while the channel for the organic phase was 50 μm deep. This difference was based on preliminary experiments, in which we found that this step height was enough to guide the two phases without compromising the contact area too much.

Ideally, pinning of the interface near the outlet occurs at the outlet junction point. In case of unpinning, the wavy wall at the end provides a new pinning point, similar to the pinning in pillar-based or array-based microfluidic devices[32,33]. This wavy wall comprises of half-circles (diameter of 5 μm) pattern starting from the outlet junction point and extends for 1 cm into each outlet channel. The joining points between two half-circles facilitate the new pinning of the interface, lowering the risk of phase contamination from one side of the channel to the other.

Microfluidic device fabrication
We fabricated our microfluidic devices using soft lithography[34]. In short, a 4-inch silicon wafer was spin-coated at 2000 rpm for 30 seconds with a negative photoresist (SU8-2050, Kayaku Advanced Materials, Inc.) and soft-baked at 100°C for 15 minutes. The thickness of this first layer of photoresist was 50 μm as determined by a profilometer (DektakXT 2, Bruker, Billerica, US). Instead of transferring the two-dimensional channel design to the coated wafer by exposing it through a patterned mask as commonly done in soft lithography, the design made in AutoCAD 2023 (Autodesk) was directly written on the coated wafer with a tabletop LaserWriter (μmLA, Heidelberg Instruments, Germany; raster scan with 1 μm laser beam at 365 nm), using an exposure dose of 300 mJ/cm^2. The patterned wafer was then post-exposure-baked at 100°C for 5 minutes. To obtain the step height, a second 50 μm thick layer of SU8-2050 photoresist was spin-coated on top of the post-exposure-baked wafer. After aligning the design of the second layer to the design of the first layer using the embedded inspection camera of the LaserWriter, the second layer was written. The wafer was then post-exposure-baked at 100°C for 5 minutes. After this second post-exposure-bake, the fully patterned wafer was developed using propylene glycol monomethyl ether acetate (Sigma-Aldrich, 99.5 %), washed with isopropyl alcohol (Sigma-Aldrich, 70 %), and hard-baked at 200°C for 20 minutes. Before its first use, the patterned wafer was silanized by exposing it to 1H,1H,2H,2H-perfluorooctyltrichlorosilane (Sigma-Aldrich, 95 %) vapour in a vacuum desiccator for one hour to prevent polydimethylsiloxane (PDMS) from sticking to the wafer.

The microfluidic devices were made from PDMS. They were prepared by mixing polymer elastomer and curing agent (Sylgard 184 Elastomer Kit, Dow Corning Comp.) in a mass ratio of 5:1. After degassing the mixture in a vacuum desiccator, it was poured over the patterned wafer in a glass 5-inch Petri dish and cured at 150°C for at least 2 hours[17]. The cured PDMS was then gently removed from the patterned wafer and cut to size. The inlets and outlets were subsequently punched using a 1.5 mm biopsy puncher. The chips were cleaned with ethanol (Sigma-Aldrich, 70 %) and dried using compressed air, before being bonded on a glass slide spin-coated with a 20 μm thick layer of PDMS (2000 rpm for 2 minutes, Laurell WS-650Mz-23NPPB) after oxygen plasma treatment for 140 seconds at 0.2-0.4 mbar (Harrick, PDC-002). The microfluidic devices were stored at 70°C for at least 12 hours before further modification to allow the PDMS to recover to its hydrophobic state.

Atmospheric pressure atomic layer deposition in microfluidic devices
To coat a thin layer of silicon oxide on the inner walls of the microfluidic channels in order to render the walls inert against the solvents used in the extraction experiments, a home-built atomic layer deposition setup was used[17,35,36]. In-channel growth of a layer of silicon oxide was achieved by sequentially flowing gas phase ALD precursors through the microchannels as described in our recent work[37]. In short, silicon tetrachloride (Alfa Aesar) was used as the metal precursor, while ozonated air (Sander Certizon) combined with deionized water was used as the oxygen precursor. A gas flow rate of 0.2 L/min was used, with the metal precursor flowing for 10 seconds and the oxygen precursor for 30 seconds, with nitrogen purges for 100 seconds in between. Each microfluidic channel was coated with 25 of such ALD cycles (i.e., the described sequence was repeated 25 times), carried out at 60°C.

Stability of parallel two-phase flow in bare and ALD-treated PDMS microfluidic devices
We studied the stability of the two-phase flow over a wide range of flow rates (0.1-150 μL/min) of the aqueous and organic solutions. As model liquids, we used a 1 M nitric acid (HNO$_3$, 65 %, Merck Sigma) solution as the aqueous phase and chloroform (CHCl$_3$, Merck Sigma) as the organic phase. While other solvents might be equally applicable, chloroform is chosen due to its ability to dissolve almost every chelator. Moreover, chloroform is a harsh solvent for PDMS, so demonstrating the nano-layer-coated microfluidic chip's resistance to chloroform supports its compatibility with a wide range of alternative solvents.

The viscosity of 1 M HNO$_3$ at 20°C is estimated to be 0.99 mPa.s (measured using a VWR falling ball viscometer, comparable with reported values in the literature[38]). The viscosity of chloroform at 20°C as provided by the supplier is 0.57 mPa.s. To estimate the interfacial tension between 1 M HNO$_3$ and chloroform, we conducted pendant drop tensiometry (Kruss easydrop) by forming a 10 μL chloroform droplet (Worthington number was ∼1[39]) in a cuvette filled with 1 M HNO$_3$. Using the Young-Laplace equation, the interfacial tension was calculated to be 31.6 mN/m, comparable to reported values in the literature[40].

The liquids were loaded in separate 5 mL syringes (Beckton-Dickinson, Discardit II) with a plastic plunger. The syringes were connected to the inlets of the microfluidic device with polytetrafluoroethylene (PTFE) tubing (outer diameter 1.6 mm, inner diameter 0.5 mm, length 300 mm, Diba, 008T16-050-200) and the liquids were driven into the device using individual syringe pumps (Harvard Apparatus Pump 11 Pico Elite Plus). The aqueous phase was injected at the inlet leading to the deeper part of the main channel, while the organic phase was injected at the inlet leading to the shallower part. Snapshots of the flow were taken using a camera (ImagingSource DFK33UX273) through an LWD plan phase 10X lens on a microscope (Euromex Oxion Inverso PLPH).

To rationalize the flow stability experiments, we compared the outcome against an available simple theoretical model[41]. In short, the transition between stable and unstable parallel flow is expected when the difference in organic and aqueous phase pressure drop over the length of the main channel due to viscous flow exceeds the difference in organic and aqueous phase pressure due to interfacial forces, known as the Laplace pressure jump. At the onset of this transition, small perturbations in the flow, for example due to the step motor of a syringe pump[42-44] lead to unpinning of the interface at the step height. The Laplace pressure jump ($\Delta P_{Laplace}$) can be estimated using the following expression[28]

$$\Delta P_{Laplace} = \frac{2\gamma \sin(\theta - 90°)}{d}, \tag{1}$$

where γ represents the interfacial tension between two liquids, θ represents the solid-liquid-liquid contact angle, and d represents the height between the ceiling of the main channel and the step (i.e., 50 μm in our work). A simple estimate of the pressure drop over the channel (ΔP_F) in both the aqueous and the organic phase is obtained through the pressure drop of a single phase flow in a rectangular channel[28,30,45], i.e.,

$$\Delta P_F = \frac{12Q\eta L}{\left(1 - 0.630\frac{d}{w}\right) d^3 w}, \tag{2}$$

where Q represents the flow rate of the considered phase, η represents the dynamic viscosity of the considered phase, L represents the length of the main channel, and d and w represent the height and width of considered phase (approximated as 100 μm × 250 μm for the aqueous phase and 50 μm × 250 μm for the organic phase. The transitions between stable and unstable parallel flow is estimated as

$$|\Delta P_{F,aqueous} - \Delta P_{F,organic}| = \Delta P_{Laplace}. \tag{3}$$

Radionuclide separation experiments

Radiotracer production and radioactivity measurements
Initial experiments were focused on the separation of La-140 from $Ba(NO_3)_2$ in Milli-Q. The radiotracers Ba-139 and La-140 were produced by neutron irradiation of BaO and La_2O_3 (Merck Sigma), respectively, at the Hoge Onderwijs Reactor (HOR) of the TU Delft Reactor Institute (the Netherlands) with a thermal neutron flux of $4.69 \cdot 10^{16}$ s^{-1}m^{-2} for 3 hours. They were subsequently dissolved in 1 M HNO_3, dried down, and redissolved in ultrapure water (Milli-Q; Merck Milli-Q Advantage A10). Ac-225 was supplied in 0.05 M HCl by Eckert & Ziegler, and Ra-223 was supplied as $^{223}RaCl_2$ (Xofigo) by GE Healthcare (Leiderdorp, the Netherlands). Ba-139, La-140, and Ra-223 were measured directly with the Wallac Wizard2 3' 2480 Automatic Gamma Counter (Perkin Elmer). Ac-225 was measured indirectly at equilibrium (> 30 minutes after experiments) through its daughter Fr-221, emitting 218 keV γ-rays. Additional experiments for the separation of Sc-46 from $Ca(NO_3)_2$ and Y-90 from $Sr(NO_3)_2$ are presented as Supplementary Information.

Solution preparation
The aqueous solutions used in the solvent extraction experiments were prepared by dissolution of different amounts of $Ba(NO_3)_2$ (Merck Sigma) in Milli-Q water and subsequent addition of radiotracers with activities of 10-15 kBq/mL. Note that for the separation of Ac-225 from Ra-223, rather than using 0.1 M $Ra(NO_3)_2$ as the (target) solution, we used 0.1 M $Ba(NO_3)_2$. This is justified by the chemical similarities of Ra and Ba, making it an often used substitute[46,47]. The organic solution used in the solvent extraction experiments contains the chelator di-2-ethylhexylphosphoric acid (D2EHPA, reagent grade < 98 %; Merck Sigma) and was prepared as a 10 %v/v D2EHPA in chloroform (Merck Sigma) solution. D2EHPA was chosen due its prior use for the separation of Sr[48], Ca[49] and La[50].

Batch solvent extraction experiments
Batch extraction experiments were performed to determine the equilibrium extraction efficiency, which is the highest possible extraction efficiency that can be obtained in the continuous-flow microfluidic experiments for a given combination of solutions and chelator. Next to these (forward) extraction experiments, also back-extraction experiments were performed to determine the optimal conditions, i.e., the lowest HCl concentration required for maximum back-extraction.

The batch forward extraction experiments were done in Eppendorf vials at a 1:1 volumetric ratio, with 0.5 mL of the aqueous and 0.5 mL of the organic solution. The vials containing both solutions were shaken on a Vortex-Genie 2 mixer (Scientific Industries, Inc.) for 1 minute at the highest speed setting, to reach equilibrium. Afterwards, the solutions were separated by pipetting and the radioactivity of both solutions was measured in order to determine the extraction efficiency. The extraction efficiency of the batch experiments ($EE\%_{batch}$) was defined as the radioactivity of the organic solution after extraction ($A_{org,out}$) relative to the radioactivity of the aqueous solution before extraction ($A_{aq,in}$), i.e.,

$$EE\%_{batch} = \frac{A_{org,out}}{A_{aq,in}} \times 100\%. \tag{4}$$

The extraction efficiency was determined for the 'produced' radionuclide as well as for the target material.

The batch back-extraction experiments were performed in a similar manner, to release the 'produced' radionuclide from the organic solutions into an aqueous solution for further use in radiopharmaceutical production. The organic solution obtained after forward extraction containing the complexed radionuclide was brought into contact with an aqueous HCl (Merck Sigma) solution. The organic and aqueous solution were pipetted into a vial at equal volumes, shaken on the Vortex mixer for 5 minutes (to ensure equilibrium even when low acid concentrations were used), and subsequently separated by pipetting. Different HCl concentrations were tested, ranging from 0-0.1 M to determine the lowest HCl concentration necessary. This might simplify the subsequent radiopharmaceutical production. The back-extraction efficiency ($BEE\%_{batch}$) was defined as the radioactivity in the resulting aqueous HCl solution ($A_{HCl,out}$) relative to the total radioactivity of the HCl and the organic solution ($A_{HCl,out} + A_{org,out}$), i.e.,

$$BEE\%_{batch} = \frac{A_{HCl,out}}{A_{HCl,out} + A_{org,out}} \times 100\%. \tag{5}$$

All batch experiments were done in triplicate and errors in the obtained values of the extraction and back-extraction efficiency were given as one standard deviation of the mean.

Microfluidic continuous-flow solvent extraction experiments
Microfluidic extraction experiments were performed in ALD-treated PDMS microfluidic chips. The aqueous, radionuclide-containing $Ba(NO_3)_2$ solution and the $D2EHPA/CHCl_3$ organic solution were loaded into 2.5 mL syringes, which were loaded on two separate syringe pumps (AL-1000 Programmable Syringe pumps 941-371-1003, World Precision Instruments, Inc.) and connected to the chips using PTFE tubing (outer diameter 1.6 mm, inner diameter 0.5 mm, length 200 mm). The extraction efficiency was studied for different contact times (0.1 - 1.8 seconds) between the two phases in the microfluidic chips. The contact times were adjusted by varying the total volumetric flow rate of the two solutions, while keeping the ratio of flow rates at 1:1. This means that the expected input/output volume of both solutions was equal although the superficial velocity of each phase differs one from another depending on their respective cross-sectional area. For simplification, the contact time t was calculated as $t = L/v$, with the length L of the main channel being equal to 11.63 mm and the average velocity v estimated from the sum of the volumetric flow rates ($Q_{aq} + Q_{org}$) over the cross-sectional channel area (S), i.e., $v = (Q_{aq} + Q_{org})/S$, with S equal to the sum area of both rectangular channel parts (deeper and shallower). At the outlet of the chip the organic solution, enriched in the 'produced' radionuclide with radioactivity $A_{org,out}$, and the aqueous solution, depleted in the 'produced' radionuclide with radioactivity $A_{aq,out}$, were collected separately and measured for their radioactivity to determine the extraction efficiency ($EE\%_{continuous}$) determined as

$$EE\%_{continuous} = \frac{A_{org,out}}{A_{aq,out} + A_{org,out}} \times 100\%. \tag{6}$$

Microfluidic back-extraction experiments were performed by injecting the organic solutions containing the 'produced' radionuclide and different aqueous HCl solutions (between 0.1 M and 4 M HCl) through microfluidic chips for contact times between 0.1 and 1.8 seconds. The aqueous solution with radioactivity $A_{HCl,out}$ and the organic solution with radioactivity $A_{org,out}$ were collected at the outlets and the continuous back-extraction efficiency ($BEE\%_{continuous}$) was determined as

$$BEE\%_{continous} = \frac{A_{HCl,out}}{A_{org,out} + A_{HCl,out}} \times 100\%. \tag{7}$$

All microfluidic experiments were done in triplicate and errors in the obtained extraction and back-extraction efficiency were given as one standard deviation of the mean.

Please note that in practice, the final processing parameters depend on the geometry of the microfluidic chip (length, width, and depth). This is determined by the chosen extraction system, the required contact time, and the stability of the parallel flow and therefore, formulation of design rules based on dimensionless number analysis helps in design and optimization of future systems.

Results and discussion
Stability of parallel two-phase flow in bare and ALD-treated PDMS microfluidic devices
Figure 2a shows the three possible flow profiles taking place in the ALD-treated PDMS microfluidic chip when using 1 M HNO_3 as the aqueous phase and $CHCl_3$ as the organic phase: stable parallel flow with the interface pinned at the step height, unstable parallel with the interface not pinned at the step height, and break-up of the parallel flow into slugs. A map of these flow profiles shows that stable parallel flow with a pinned interface (filled squares) is obtained for a relatively wide range of flow rate combinations, see Fig. 2b. This window of stable operation is much larger than in microfluidic chips without the guiding structure[29–31], especially at a low flow rate, indicating the importance of the guiding structure. For the larger flow rates studied in this work, parallel flow is still observed, but with the interface not pinned to the step height over the full length of the microchannel (open squares). For this flow profile, we observe occasional break-up of the unpinned interface into slugs. For
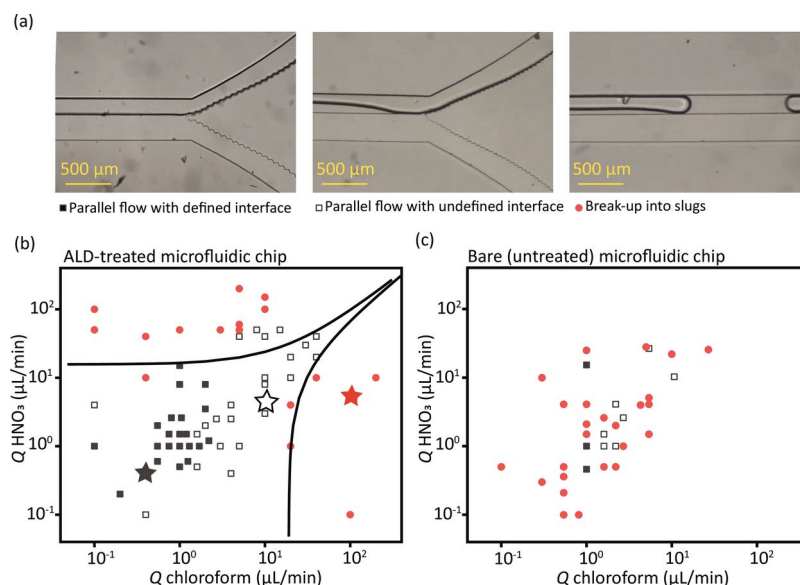
Fig. 2. (**a**) Optical microscopy photos taken in an ALD-treated PDMS microfluidic chip, illustrating the three types of two-phase flow observed at different combinations of the flow rate of the aqueous and organic solution. The solution in the upper and lower half of the channel is 1 M HNO_3 and $CHCl_3$, respectively. (**b**) Flow map of 1 M HNO_3 and $CHCl_3$ inside ALD-treated PDMS microfluidic chips (n=3). The stars correspond to the photos shown in (**a**). The lines represent the calculated transition between stable and unstable parallel flow using Equations 1–3. (**c**) Flow map of 1 M HNO_3 and $CHCl_3$ inside a bare (untreated) microfluidic chip (n=1).

the highest flow rate ratios, the unpinned interface breaks-up downstream the Y-junction and slug flow (red circles) is observed. The transition between parallel flow with (partly) pinned interface (squares) and slug flow, represented by the solid lines, is reasonably well captured by the simple model (Equations 1–3).

For reference, we attempted to perform the same measurements in a bare (untreated) microfluidic chip. As expected, during these experiments, many chips leaked due to the swelling and deformation of PDMS under exposure to organic solvents[51]. The employed $CHCl_3$ induces matrix swelling inside the microfluidic channel, estimated at around 1.39 (length swelling ratio[18]). Swelling also reduces the channel space, leading to an undefined flow profile. While the experiments in ALD-treated chips were reproducible, we observed strong variations from experiment to experiment in untreated chips. An example experiment in a single untreated chip is shown in Fig. 2c, illustrating the importance of the silicon oxide nano-layer of the ALD-treated chip to increases the organic solvent resistance of PDMS by preventing direct contact between the organic solvent and PDMS, as further detailed in our earlier work[17,37].

Visual inspection of the organic and aqueous solutions after parallel flowing in the microfluidic chip showed no droplets in both phases, indicating the complete phase separation of the two solutions.

Batch solvent extraction

Batch extraction of La-140 (simulated 'produced' radionuclide) from Ba (simulated target material) and of Ac-225 from Ra-223 (in 0.1 M $Ba(NO_3)_2$) showed high extraction efficiencies (> 98 %) for all tested solutions, see Fig. 3a. With a mixing time of (less than) 1 minute, the complexation of D2EHPA is considered very fast. Simultaneously, co-extraction of the target material into the organic phase remained low in all solutions: below 2 % for Ba-139 and below 0.3 % for Ra-223. In practice, the co-extraction percentage in the final solution can even be further lowered using a second, commonly employed purification step, although it is outside the scope of this proof-of-principle study. It should also be noted that the aqueous solution did not consist purely of Ra, but a Ra-223 tracer dissolved in a 0.1 M $Ba(NO_3)_2$ solution (commonly written as $[^{223}Ra]Ba(NO_3)_2$). Because of the chemical similarities of group 2 and 3 elements, we additionally conducted extraction experiments for the separation of Y from Sr and Sc from Ca, which can be found in the Supplementary Information. All the extractions also show considerably high efficiency (> 80 %), as expected.

Back-extraction experiments show back-extraction efficiencies over 98 % for both La-140 and Ac-225 (as well as for Ba-139 and Ra-223) when using 0.1 M HCl, see Fig. 3b. These efficiencies decrease with decreasing HCl concentration. When using 0.01 M HCl as back-extraction solution, the back-extraction efficiency is significantly higher for Ac-225 compared to La-140. These results indicate a higher complex stability of ^{140}La-D2EHPA over ^{225}Ac-D2EHPA. The complex stability is dependent on the electronegativity and the ionic size and therefore, on the charge density, resulting in a lower complex stability for the larger Ac. This trend of decreasing complex stability with decreasing charge density is often found in chelate complexation[52] and was shown for La and Ac before[53]. Our back-extraction results, including the results shown in the Supplementary Information for the separation of Y from Sr and Sc from Ca, are in line with this trend.
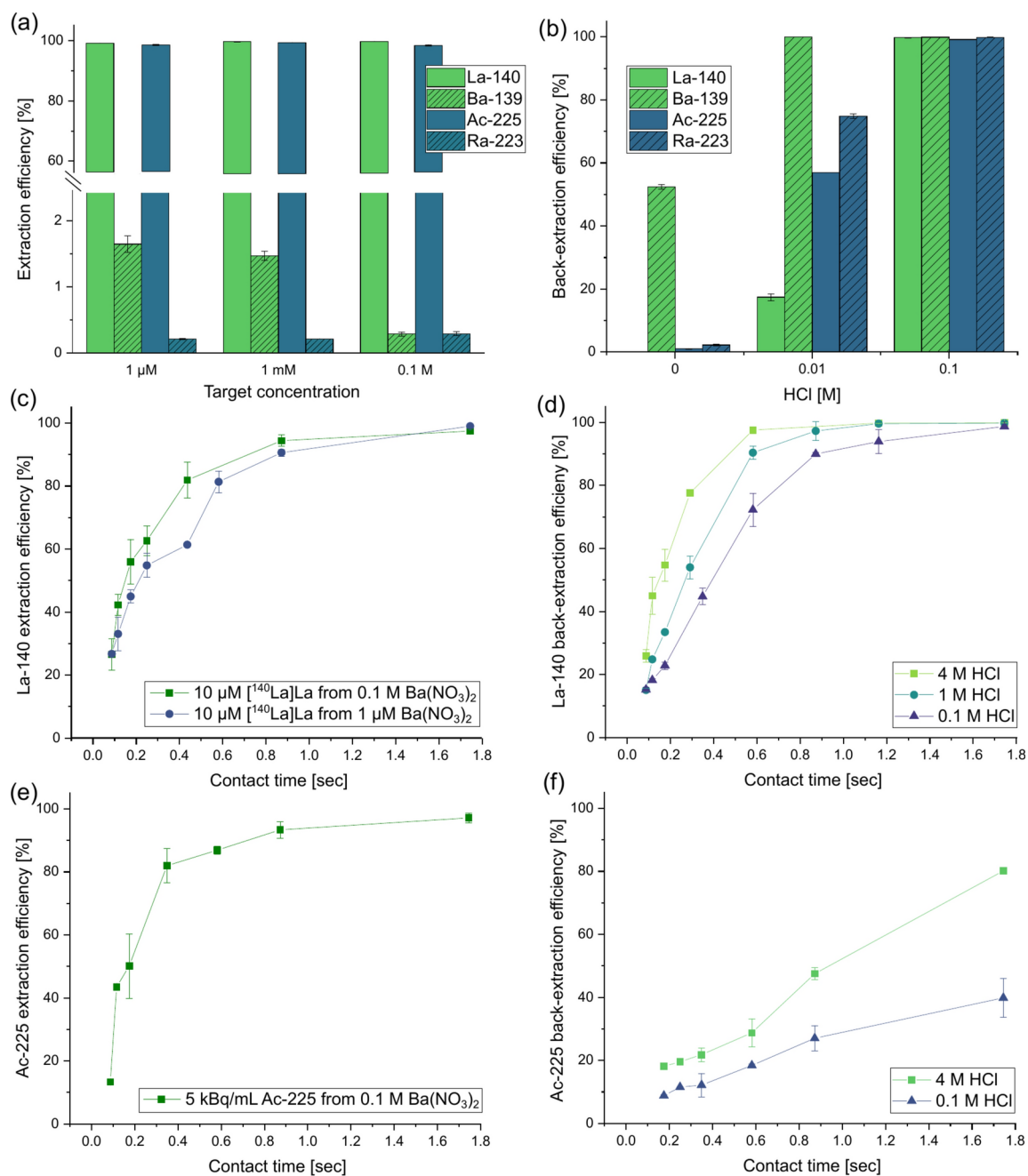
Fig. 3. (**a**) Batch extraction of Ba-139, La-140, Ac-225, and Ra-223 for varying target concentrations. (**b**) Batch back-extraction of Ba-139, La-140, Ac-225, and Ra-223 for varying HCl concentrations. (**c**) Microfluidic extraction of La-140 from two different $Ba(NO_3)_2$ solutions for varying contact times. (**d**) Microfluidic back-extraction of La-140 into different HCl solutions for varying contact times. (**e**) Microfluidic extraction of Ac-225 from 0.1 M $Ba(NO_3)_2$ solutions for varying contact times. (**f**) Microfluidic back-extraction of Ac-225 into different HCl solutions for varying contact times. All experiments were done in triplicate and error bars represent the standard deviation of the mean.

Microfluidic continuous-flow solvent extraction

The batch experiments were instrumental in determining the maximum achievable extraction efficiency with the continuous-flow microfluidic experiments. We used the insights from the batch experiments to design and perform the microfluidic (forward) extraction experiments with (target) solution concentrations of 0.1 M $Ba(NO_3)_2$ and 1 μM $Ba(NO_3)_2$ in Milli-Q for La-140 and 0.1 M $Ba(NO_3)_2$ for Ac-225. Additionally, the back-extraction experiments were designed and performed with HCl solutions with concentrations higher than 0.1 M. For La-140 extraction from the 0.1 M and 1 μM $Ba(NO_3)_2$ solutions, the extraction efficiency for the longest contact time (1.7 seconds) was 97.4 % $\pm$ 0.7 % and 99.0 % $\pm$ 0.2 %, respectively, see Fig. 3c. For Ac-225

extraction from the 0.1 M Ba(NO$_3$)$_2$ solution, a comparable extraction efficiency of 97.2 % ± 1.5 % was obtained for the same contact time, see Fig. 3e.

The speed of extraction is slightly influenced by the target concentration, as seen from the two curves in Fig. 3c, which are different in target concentration by 5 orders of magnitude. The salting-out-effect, usually increasing extraction efficiency and separation because of a higher ionic strength of the solution, only has a minor influence on the results. A comparison of the curves in Fig. 3c and e suggests that the speed of extraction is insensitive to the radionuclide concentration, which is six orders of magnitude higher for La-140 than for Ac-225. Usually, the metal concentration (both radionuclide and target) plays a major role during the extraction in a microfluidic device because the concentration drives the diffusive flux[54]. Our results indicate that the concentration of the radiometal that is to be extracted does not have a large influence on the extraction when using D2EHPA. Others have shown before that the D2EHPA concentration and its reaction kinetics have the highest influence on the extraction speed[55,56]. Based on the molecular structure of D2EHPA illustrated in Fig. 4a, Sun et al. (2021)[57] proposed that D2EHPA first transfers into the aqueous phase where it forms a complex with the product radionuclide, which subsequently transfers into the organic phase, see Fig. 4b, shortening the diffusion distance of the radiometal. These steps, including the electrostatic pull of D2EHPA towards the metal ions[58], influence the extraction speed. While the full set of Ac-225 extraction experiments was performed with fixed radionuclide and target concentrations, we expect based on the aforementioned reasons that the Ba (or Ra) target concentration and the Ac-225 concentration have no major influence on Ac-225 extraction.

The back-extraction efficiency of La-140 into 0.1 M, 1 M, and 4 M HCl solutions exceeded 99 % within 1.7 seconds of contact time, see Fig. 3d. The back-extraction efficiency of Ac-225 with the same contact time is considerably lower, i.e., 80 % ± 1 % and 40 % ± 6 % for extraction into 4 M and 0.1 M HCl solutions, respectively, see Fig. 3f. While the speed of back-extraction depends on the used HCl concentration, the extraction efficiency plateaus within 1.7 seconds for all three used HCl concentrations for La-140. For Ac-225, the plateau is not visible within 1.7 seconds. A comparison of the La-140 and Ac-225 back-extraction experiments for the same HCl concentrations suggests that the concentration of the radionuclide/D2EHPA complex has a higher influence on the back-extraction speed compared to the speed of the (forward) extraction. This implies that diffusion plays a more prominent role in back-extraction. Additionally, the now-neutral charge of the complex does not offer the ability of electrostatic pull of the complex near the interface. Therefore, the movement to the interface is slower. An increase in the back-extraction efficiency of Ac-225 could likely be accomplished by increasing the HCl concentration or increasing the contact time.

Overall, excellent extraction and back-extraction efficiencies can be achieved with the developed microfluidic solvent extraction method for both La-140 (97.4 % ± 0.7 % and 99.8 % ± 0.1 %, respectively) and Ac-225 (97.2 % ± 1.5 % and 80.1 % ± 0.7 %, respectively). Ac-225 currently receives enormous attention for its potential in targeted alpha therapy. Other commonly used methods for the separation of Ac-225 include the use of ion-exchange column chromatography[3,59,60], microfluidic ion-exchange[61], or solvent impregnated resins[62]. While achieving comparable results for the total recovery (the combination of extraction and back-extraction efficiency) of Ac-225, the developed microfluidic solvent extraction method exceeds the above-mentioned methods in terms of minimizing chemical volumes[59,60,62], reducing the acidity of the final solution[59,61,62], or lowering processing time to only a few minutes, depending on the size and number of microfluidic chips[61,62], as well as the total volume of the radionuclide-containing solution. Thus, the developed microfluidic solvent extraction of Ac-225 presents a promising alternative to conventional separation methods. The newly developed nano-layer coated PDMS microfluidic chip with a step-height and wavy outlet geometry solves the issue of insufficient phase separation and unstable parallel flow in microfluidic chips, and enables the future use and automation of solvent extraction for the separation of medical radionuclides.

Conclusion

We developed a microfluidic PDMS-based chip for fast, continuous, and efficient solvent extraction of radionuclides. To overcome the general issue that PDMS is incompatible with common organic solvents used in solvent extraction experiments, we used our recently developed atomic layer deposition method to deposit a layer of silicon oxide on the inside of the microchannels, rendering them inert. Two key features incorporated
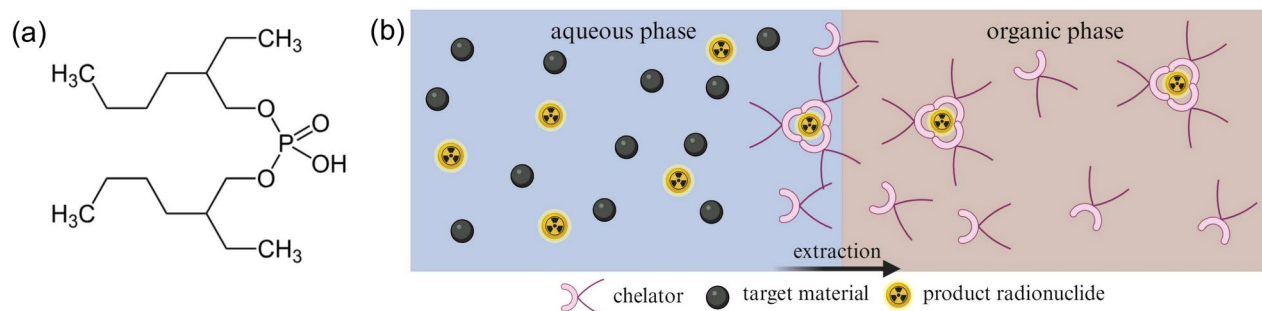
Fig. 4. (**a**) Structure of D2EHPA. (**b**) Illustration of the extraction mechanism proposed by Sun et al.[57] showing that D2EHPA transfers into the aqueous phase where it forms a complex with the product radionuclide, which subsequently transfers into the organic phase.

in the microfluidic chip, a difference in height in the channel for the organic and aqueous phase and a wavy wall near the exit, proved essential to obtain a stable parallel flow and a near-perfect separation of the phases at the exit. With the newly designed microfluidic chip and using the chelator D2EHPA in chloroform as the organic solution, a high extraction efficiency of 97.2 % $\pm$ 1.5 % of Ac-225 was accomplished in less than 1.8 seconds of contact time, while only co-extracting a maximum of 0.293 % $\pm$ 0.034 % of Ra, according to batch experiments. Back-extraction can be achieved in 0.1 M HCl, where increasing the contact time or the HCl concentration was found to speed up the back-extraction process. The presented proof-of-concept showcases the potential of microfluidic chips, for fast, continuous, and potentially automatable liquid-liquid extraction for the separation of medical radionuclides.

Data availability

The datasets used and/or analyzed during the current study are available from the corresponding author on reasonable request.

References

1. https://world nuclear.org. Radioisotopes in medicine (Accessed April 2024) .
2. Qaim, S. M. & Spahn, I. Development of novel radionuclides for medical applications. *J. Labell. Compd. Radiopharm.* **61**, 126–140. https://doi.org/10.1002/jlcr.3578 (2018).
3. Robertson, A. K. H., Ramogida, C. F., Schaffer, P. & Radchenko, V. Development of ^{225} Ac radiopharmaceuticals: Triumf perspectives and experiences. *Curr. Radiopharm.* **11**, 156–172. https://doi.org/10.2174/1874471011666180416161908 (2018).
4. Boersma, H. H. GMP in radiopharmacy: The current situation in its context. In *Nuclear Medicine and Molecular Imaging: Basic Concepts, Radiopharmacy and Instrumentation* (ed. Boersma, H. H.) 243–249 (Elsevier, 2022).
5. Martini, P. et al. Perspectives on the use of liquid extraction for radioisotope purification. *Molecules* **24**, 334. https://doi.org/10.3390/molecules24020334 (2019).
6. Ramogida, C. F. et al. Evaluation of polydentate picolinic acid chelating ligands and an alpha-melanocyte-stimulating hormone derivative for targeted alpha therapy using ISOL-produced ^{225} Ac. *EJNMMI Radiopharm. Chem.*[SPACE]https://doi.org/10.1186/s41181-019-0072-5 (2019).
7. Pedersen, K. S., Nielsen, K. M., Fonslet, J., Jensen, M. & Zhuravlev, F. Separation of radiogallium from zinc using membrane-based liquid-liquid extraction in flow: Experimental and cosmo-rs studies. *Solvent Extract. Ion Exchange* **37**, 376–391. https://doi.org/10.1080/07366299.2019.1646982 (2019).
8. Trapp, S. et al. Membrane-based microfluidic solvent extraction of Ga-68 from aqueous zn solutions: towards an automated cyclotron production loop. *EJNMMI Radiopharm. Chem.* **8**, 9. https://doi.org/10.1186/s41181-023-00195-2 (2023).
9. Chakravarty, R. et al. Microfluidic solvent extraction of no-carrier-added ^{64} Cu from irradiated Zn target for radiopharmaceutical preparation. *Chem. Eng. J. Adv.* **13**, 100433. https://doi.org/10.1016/j.ceja.2022.100433 (2023).
10. Helle, G., Mariet, C. & Cote, G. Microfluidic tools for the liquid-liquid extraction of radionuclides in analytical procedures. *Procedia Chem.* **7**, 679–684. https://doi.org/10.1016/j.proche.2012.10.103 (2012).
11. Mariet, C. et al. Microfluidics devices applied to radionuclides separation in acidic media for the nuclear fuel cycle. *Micro Nano Eng.* **3**, 7–14. https://doi.org/10.1016/j.mne.2019.02.006 (2019).
12. Abdollahi, P., Karimi-Sabet, J., Moosavian, M. A. & Amini, Y. Microfluidic solvent extraction of calcium: Modeling and optimization of the process variables. *Sep. Purif. Technol.* **231**, 115875. https://doi.org/10.1016/j.seppur.2019.115875 (2020).
13. Whitesides, G. M. The origins and the future of microfluidics. *Nature* **442**, 368–373. https://doi.org/10.1038/nature05058 (2006).
14. Liu, Q., Huang, W., Liu, B., Wang, P.-C. & Chen, H.-B. Gamma radiation chemistry of polydimethylsiloxane foam in radiation-thermal environments: experiments and simulations. *ACS Appl. Mater. Interfaces* **13**, 41287–41302. https://doi.org/10.1021/acsami.1c10765 (2021).
15. Victor, A. et al. Study of PDMS characterization and its applications in biomedicine: A review. *J. Mech. Eng. Biomech.* **4**, 1–9. https://doi.org/10.24243/JMEB/4.1.163 (2019).
16. Ren, K., Zhou, J. & Wu, H. Materials for microfluidic chip fabrication. *Acc. Chem. Res.* **46**, 2396–2406. https://doi.org/10.1021/ar300314s (2013).
17. Santoso, A., Damen, A., van Ommen, J. R. & van Steijn, V. Atmospheric pressure atomic layer deposition to increase organic solvent resistance of PDMS. *Chem. Commun.* **58**, 10805–10808. https://doi.org/10.1039/D2CC02402K (2022).
18. Lee, J. N., Park, C. & Whitesides, G. M. Solvent compatibility of poly (dimethylsiloxane)-based microfluidic devices. *Analyt. Chem.* **75**, 6544–6554. https://doi.org/10.1021/ac0346712 (2003).
19. Van Bui, H., Grillo, F. & Van Ommen, J. Atomic and molecular layer deposition: off the beaten track. *Chem. Commun.* **53**, 45–71. https://doi.org/10.1039/C6CC05568K (2017).
20. Vulto, P. et al. Phaseguides: a paradigm shift in microfluidic priming and emptying. *Lab Chip* **11**, 1596–1602. https://doi.org/10.1039/C0LC00643B (2011).
21. Kratochwil, C. et al. ^{225} Ac- PSMA-617 for psma-targeted a-radiation therapy of metastatic castration-resistant prostate cancer. *J. Nucl. Med.* **57**, 1941–1944. https://doi.org/10.2967/jnumed.116.178673 (2016).
22. Anderson, P. M., Subbiah, V. & Trucco, M. M. Current and future targeted alpha particle therapies for osteosarcoma: Radium-223, actinium-225, and thorium-227. *Front. Med.* **9**, 1030094. https://doi.org/10.3389/fmed.2022.1030094 (2022).
23. Mastren, T. et al. Simultaneous separation of actinium and radium isotopes from a proton irradiated thorium matrix. *Sci. Rep.* **7**, 8216. https://doi.org/10.1038/s41598-017-08506-9 (2017).
24. Engle, J. W. The production of Ac-225. *Curr. Radiopharm.* **11**, 173–179. https://doi.org/10.2174/1874471011666180418141357 (2018).
25. Apostolidis, C. et al. Cyclotron production of Ac-225 for targeted alpha therapy. *Appl. Radiat. Isot.* **62**, 383–387. https://doi.org/10.1016/j.apradiso.2004.06.013 (2005).
26. Nagatsu, K. et al. Cyclotron production of ^{225} Ac from an electroplated ^{226} Ra target. *Eur. J. Nucl. Med. Mol. Imaging* **49**, 279–289. https://doi.org/10.1007/s00259-021-05460-7 (2021).
27. Melville, G. & Allen, B. J. Cyclotron and linac production of Ac-225. *Appl. Radiat. Isotopes* **67**, 549–555. https://doi.org/10.1016/j.apradiso.2008.11.012 (2009).
28. Hibara, A. et al. Surface modification method of microchannels for gas- liquid two-phase flow in microchips. *Anal. Chem.* **77**, 943–947. https://doi.org/10.1021/ac0490088 (2005).
29. Pohar, A., Lakner, M. & Plazl, I. Parallel flow of immiscible liquids in a microreactor: modeling and experimental study. *Microfluid. Nanofluid.* **12**, 307–316. https://doi.org/10.1007/s10404-011-0873-7 (2012).
30. Bruus, H. *Theoretical Microfluidics* Vol. 18 (Oxford University Press, 2007).

31. Hibara, A., Fukuyama, M., Chung, M., Priest, C. & Proskurnin, M. A. Interfacial phenomena and fluid control in micro/nanofluidics. *Anal. Sci.* **32**, 11–21. https://doi.org/10.2116/analsci.32.11 (2016).
32. Saha, A. A. & Mitra, S. K. Effect of dynamic contact angle in a volume of fluid (VOF) model for a microfluidic capillary flow. *J. Colloid Interface Sci.* **339**, 461–480. https://doi.org/10.1016/j.jcis.2009.07.071 (2009).
33. Gumuscu, B., Bomer, J. G., van den Berg, A. & Eijkel, J. C. Large scale patterning of hydrogel microarrays using capillary pinning. *Lab Chip* **15**, 664–667. https://doi.org/10.1039/C4LC01350F (2015).
34. Duffy, D. C., McDonald, J. C., Schueller, O. J. & Whitesides, G. M. Rapid prototyping of microfluidic systems in poly (dimethylsiloxane). *Anal. Chem.* **70**, 4974–4984. https://doi.org/10.1021/ac980656z (1998).
35. Santoso, A. et al. Robust surface functionalization of PDMS through atmospheric pressure atomic layer deposition. *Atomic Layer Depos.* **1**, 1–13. https://doi.org/10.3897/aldj.1.105146 (2023).
36. Goulas, A. & Van Ommen, J. R. Atomic layer deposition of platinum clusters on Titania nanoparticles at atmospheric pressure. *J. Mater. Chem. A* **1**, 4647–4650. https://doi.org/10.1039/C3TA01665J (2013).
37. Santoso, A., David, M. K., Boukany, P. E., van Steijn, V. & van Ommen, J. R. Atmospheric pressure atomic layer deposition for in-channel surface modification of pdms microfluidic chips. *Chem. Eng. J.*[SPACE]https://doi.org/10.1016/j.cej.2024.155269 (2024).
38. Sohnel, O. & Novotny, P. *Densities of Aqueous Solutions of Inorganic Substances* (Elsevier, 1985).
39. Berry, J. D., Neeson, M. J., Dagastine, R. R., Chan, D. Y. & Tabor, R. F. Measurement of surface and interfacial tension using pendant drop tensiometry. *J. Colloid Interface Sci.* **454**, 226–237. https://doi.org/10.1016/j.jcis.2015.05.012 (2015).
40. Demond, A. H. & Lindner, A. S. Estimation of interfacial tension between organic liquids and water. *Environ. Sci. Technol.* **27**, 2318–2331. https://doi.org/10.1021/es00048a004 (1993).
41. Kralj, J. G., Sahoo, H. R. & Jensen, K. F. Integrated continuous microfluidic liquid-liquid extraction. *Lab Chip* **7**, 256–263. https://doi.org/10.1039/B610888A (2007).
42. Baeckert, M. et al. Performance of modern syringe infusion pump assemblies at low infusion rates in the perioperative setting. *Br. J. Anaesth.* **124**, 173–182. https://doi.org/10.1016/j.bja.2019.10.007 (2020).
43. Li, Z., Mak, S. Y., Sauret, A. & Shum, H. C. Syringe-pump-induced fluctuation in all-aqueous microfluidic system implications for flow rate accuracy. *Lab Chip* **14**, 744–749. https://doi.org/10.1039/C3LC51176F (2014).
44. Korczyk, P. M., Cybulski, O., Makulska, S. & Garstecki, P. Effects of unsteadiness of the rates of flow on the dynamics of formation of droplets in microfluidic systems. *Lab Chip* **11**, 173–175. https://doi.org/10.1039/C0LC00088D (2011).
45. Amini, Y. et al. Computational fluid dynamics simulation of two-phase flow patterns in a serpentine microfluidic device. *Sci. Rep.* **13**, 9483. https://doi.org/10.1038/s41598-023-36672-6 (2023).
46. Brown, M. A. Metal oxide sorbents for the separation of radium and actinium. *Ind. Eng. Chem. Res.* **59**, 20472–20477. https://doi.org/10.1021/acs.iecr.0c04084 (2020).
47. Toro-González, M., Dame, A. N., Mirzadeh, S. & Rojas, J. V. Encapsulation and retention of 225ac, 223ra, 227th, and decay daughters in zircon-type gadolinium vanadate nanoparticles. *Radiochim. Acta* **108**, 967–977. https://doi.org/10.1515/ract-2019-3206 (2020).
48. Naik, P. et al. Separation of carrier-free 90Y from 90Sr by SLM technique using D2EHPA in N-dodecane as carrier. *Sep. Sci. Technol.* **45**, 554–561. https://doi.org/10.1080/01496390903484925 (2010).
49. Cao, X., Zhang, T.-A., Zhang, W. & Lv, G. Solvent extraction of Sc(iii) by D2EHPA/TBP from the leaching solution of vanadium slag. *Metals*[SPACE]https://doi.org/10.3390/met10060790 (2020).
50. Nascimento, M. et al. Separation of rare earths by solvent extraction using DEHPA. *Rem Revista Escola de Minas* **68**, 427–434. https://doi.org/10.1590/0370-44672015680140 (2015).
51. Dangla, R., Gallaire, F. & Baroud, C. N. Microchannel deformations due to solvent-induced PDMS swelling. *Lab Chip* **10**, 2972–2978. https://doi.org/10.1039/C003504A (2010).
52. Chapman, D. Electronegativity and the stability of metal complexes. *Nature* **174**, 887–888. https://doi.org/10.1038/174887a0 (1954).
53. Mishustin, A. Estimate of the stability constants of trivalent actinide and lanthanide complexes with o-donor ligands in aqueous solutions. *Russ. J. Inorg. Chem.* **55**, 746–752. https://doi.org/10.1134/S0036023610050141 (2010).
54. Holden, M. A., Kumar, S., Castellana, E. T., Beskok, A. & Cremer, P. S. Generating fixed concentration arrays in a microfluidic device. *Sens. Actuat. B Chem.* **92**, 199–207. https://doi.org/10.1016/S0925-4005(03)00129-1 (2003).
55. Amiliana, R. A. Extraction of Yttrium from Nd Hydroxide concentrate by using D2EHPA. *J. Phys. Conf. Ser.* **1436**, 012002. https://doi.org/10.1088/1742-6596/1436/1/012002 (2020).
56. Starý, J. *The Solvent Extraction of Metal Chelates* (Pergamon, 1964).
57. Sun, P. et al. Antagonistic role of aqueous complexation in the solvent extraction and separation of rare earth ions. *ACS Cent. Sci.* **7**, 1908–1918. https://doi.org/10.1021/acscentsci.1c00960 (2021).
58. Jing, Y. et al. Deep insights into the solution and interface behaviors in heavy rare earth extraction: A molecular dynamics study. *J. Mol. Liq.* **296**, 111790. https://doi.org/10.1016/j.molliq.2019.111790 (2019).
59. Fitzsimmons, J. et al. Optimization of cation exchange for the separation of actinium-225 from radioactive thorium, radium-223 and other metals. *Molecules* **24**, 1921. https://doi.org/10.3390/molecules24101921 (2019).
60. Zielinska, B., Apostolidis, C., Bruchertseifer, F. & Morgenstern, A. An improved method for the production of Ac-225/ Bi-213 from Th-229 for targeted alpha therapy. *Solvent Extr. Ion Exchange* **25**, 339–349. https://doi.org/10.1080/07366290701285108 (2007).
61. Davern, S. et al. Microfluidics-based separation of actinium-225 from radium-225 for medical applications. *Sep. Sci. Technol.* **54**, 1994–2002. https://doi.org/10.1080/01496395.2019.1614956 (2019).
62. Friend, M. T. et al. Extraction chromatography of [225] Ac and lanthanides on n, n-dioctyldiglycolamic acid/1-butyl-3-methylimidazolium bis (trifluoromethylsulfonyl) imide solvent impregnated resin. *J. Chromatogr. A* **1624**, 461219. https://doi.org/10.1016/j.chroma.2020.461219 (2020).

Acknowledgements

Author contributions

Concept and design of the study (S.T., A.S., E.P., J.R.v.O., V.v.S., and R.M.d.K.); acquisition and analysis of data (S.T., A.S., and Y.H.); drafting a significant portion of the manuscript or figures (S.T., A.S., J.R.v.O., V.v.S., and R.M.d.K.)

Declarations

Competing interests
The authors declare no competing interests.

Additional information
Supplementary Information The online version contains supplementary material available at https://doi.org/10.1038/s41598-024-81177-5.

Correspondence and requests for materials should be addressed to V.v.S. or R.M.d.K.

Reprints and permissions information is available at www.nature.com/reprints.

Publisher's note Springer Nature remains neutral with regard to jurisdictional claims in published maps and institutional affiliations.